Motion Characteristics Analysis of a Novel Spherical Two-degree-of-freedom Parallel Mechanism

Chen Ziming
Yanshan University
Chen Xuechan
Yanshan University
Gao Min
Yanshan University
Zhao Chen
Yanshan University
Zhao Kun
Yanshan University
Li Yanwen (ywl@ysu.edu.cn)
Yanshan University

Original Article

Keywords: spherical parallel mechanism, 2DOF, workspace, motion planning

Posted Date: March 3rd, 2021

DOI: https://doi.org/10.21203/rs.3.rs-258461/v1

Motion characteristics analysis of a novel spherical two-degree-of-freedom parallel mechanism

Ziming Chen, School of Mechanical Engineering, Yanshan University, Qinhuangdao, Hebei 066004, China
E-mail:chenzm@ysu.edu.cn

Xuechan Chen, School of Mechanical Engineering, Yanshan University, Qinhuangdao, Hebei 066004, China
E-mail:chenxuechan@foxmail.com

Min Gao, School of Mechanical Engineering, Yanshan University, Qinhuangdao, Hebei 066004, China
E-mail: gm@stumail.ysu.edu.cn

Chen Zhao, School of Mechanical Engineering, Yanshan University, Qinhuangdao, Hebei 066004, China
E-mail: zchen@stumail.ysu.edu.cn

Kun Zhao, School of Mechanical Engineering, Yanshan University, Qinhuangdao, Hebei 066004, China
E-mail: ysuzhaok@foxmail.com

Yanwen Li, School of Mechanical Engineering, Yanshan University, Qinhuangdao, Hebei 066004, China
E-mail: ywl@ysu.edu.cn

Corresponding author：Yanwen Li　E-mail：ywl@ysu.edu.cn

Motion characteristics analysis of a novel spherical two-degree-of-freedom parallel mechanism

CHEN Ziming, CHEN Xuechan, GAO Min, ZHAO Chen, ZHAO Kun, and LI Yanwen*

Parallel Robot and Mechatronic System Laboratory of Hebei Province, Yanshan University, Qinhuangdao, Hebei 066004, China

Abstract: In this paper, a novel two-degree-of-freedom (2DOF) spherical parallel mechanism(SPM) with symmetrical structure is proposed and analyzed. First, the models of forward kinematics and inverse kinematics are established based on D-H parameters, and the Jacobian matrix of the mechanism is obtained and verified. Second, the workspace of the mechanism is obtained according to inverse kinematics and link interference conditions. Next, rotational characteristics analysis shows that the end effector can achieve continuous rotation about an axis located in the mid-plane and passing through the rotation center of the mechanism. Moreover, the rotational characteristics of the mechanism are proved and motion planning is carried out. A numerical example is given to verify the kinematics analysis and motion planning. Finally, some variant mechanisms can be synthesized. This work lays the foundation for the motion control and practical application of this 2DOF SPM.

Keywords: spherical parallel mechanism, 2DOF, workspace, motion planning

1 Introduction

Spherical Parallel Mechanism (SPM) is a special spatial parallel mechanism. Its end effector can rotate freely around the point. The SPM has important application value and has been widely used, such as the azimuth tracking system[1], the bionic robot[2], surgical robot[3], and the medical device[4].The research about SPM mostly focuses on 2DOF SPM[5] and 3DOF SPM[6]. The theoretical research and practical application of 3DOF SPM are quite mature. For example, theoretical research about the typical 3-RRR 3DOF SPM has been studied in terms of its working space[7], singularity[8], dexterity[9], stiffness[10], dynamics[11]. And in practical engineering applications, Gosselin proposed the famous agile eye in 1994[12], and Houssem Saafi et al. made a research on the haptic medical device[4], etc. In most cases, the 2DOF SPM can satisfy application requirements, such as pointing mechanisms[13] used in spherical engraving machines, azimuth tracking of satellite antennas, and automatic ground tracking equipment for various aircraft, etc., and some 2DOF artificial wrists sorted out by Bajaj[14].

The representative 2DOF SPM is the spherical 5R mechanism. Ouerfelliz studied the direct and inverse kinematics[15], kinematic and dynamic optimization of a general spherical 5R linkage. Cervantes-Sanchez analyzed its workspace and singularity[16]. Zhang et al. had a further analysis of the workspace of spherical 5R mechanism and spherical 2DOF parallel mechanism with actuation redundancy[17], as well as dynamic analysis[18,19], trajectory planning[20] and parameter optimization[21]. Yu et al. introduced[22] a simple and visual graphic method for mobility analysis of parallel mechanisms and presented a novel 2DOF rotational parallel mechanism derived from well-known Omni Wrist III. Dong et al. analyzed[23] the kinematics, singularity and workspace of a class of 2DOF rotational parallel manipulators in geometric approach. Chen et al. proposed[24] a new geometric kinematic modeling approach based on the concept of instantaneous single-rotation-angle and used for the 2DOF RPMs with symmetry in a homo-kinetic plane. Kim et al. deformed the spherical 5R mechanism[25], designed the spatial self-adaptive finger clamp, and conducted constraint analysis, optimization design of the

structure and grasping experiment on it. Xu et al. established a theory regarding the type synthesis of the two-rotational-degrees-of-freedom parallel mechanism with two continuous rotational axes systematically[26]. Terence et al. conducted the decoupling design of 5R spherical mechanism and compared it with traditional 5R spherical mechanism in motion characteristics and workspace[27]. Cao et al. obtained a three-rotation, one-translation (3R1T) manipulator for minimally invasive surgery by connecting the revolute pair and the prismatic pair to a 2DOF spherical mechanism[28], and analyzed its kinematics and singularity. Alamdar et al. introduced a new non-symmetric 5R-SPM and developed a geometrical approach to analyze its configurations and singularities[29].

In this paper, we propose a novel 2DOF SPM with symmetrical structure and its variant Mechanism. The article is organized as follows: Sec.2 provides a description of the proposed SPM's structure, analysis of its mobility, the models of forward kinematics and inverse kinematics are established, and the Jacobian matrix of the mechanism is obtained and verified. In Sec.3, the workspace of the mechanism is obtained. The rotation characteristics of SMP are analyzed in Sec.4. Sec.5 describes variant mechanism of the 2DOF SPM. Finally, the conclusions are drawn.

2 Kinematics Analysis of the 2DOF SPM

2.1 Mobility Analysis

The schematic diagram of the 2DOF SPM is shown in Fig. 1, all the revolute axes intersect at one-point O, called the rotation center of the mechanism. The base is connected with the end effector by three spherical serial 3R sub-chains: $B_1B_2B_3$, $B_4B_5B_6$ and $B_7B_8B_9$. There is a special spherical sub-chain consisting of link 9, link 10 and component 11 and connected by two arc prismatic pairs, limits the revolute axes OB_2, OB_5 and OB_8 on a plane, which is defined as the mid-plane of the mechanism. And the spherical 3R sub-chains $B_7B_8B_9$ and component 11 forming a symmetric double arc slider-rocker mechanism aims at keeping the mid-plane always coplanar with the angular bisector of spherical angle $\angle B_1B_2B_3$ [30], ensuring the base and the end effector are symmetric with respect to the mid-plane during the movement of the mechanism.

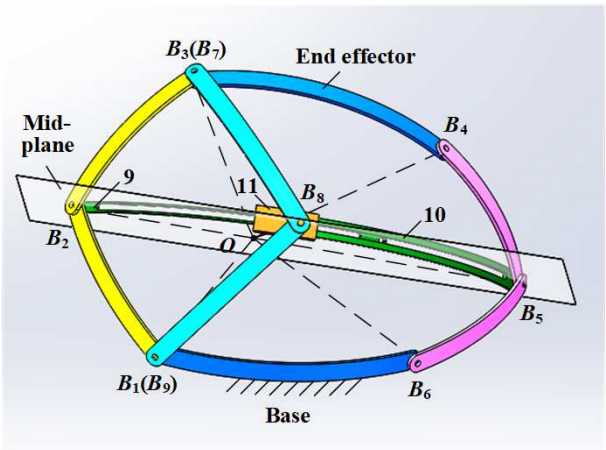

Fig. 1. Schematic diagram of the 2-DOF SPM

The DOF of the mechanism can be calculated by using the G-K formula:

$$M = d(n - g - 1) + \sum_{i=1}^{g} f_i \tag{1}$$

where d is the order of a mechanism (for the spherical mechanism d=3), n is the number of components including the base, g is the number of kinematic pairs, f_i is the freedom of the i-th

kinematic pair. For this mechanism n=11, g=14, and $\sum f_i$=14. Therefore, the mechanism has 2DOFs.

2.2 Inverse Kinematics of the SPM

2.2.1 Establishment of the coordinate systems

As shown in Fig. 2, a global coordinate system O-$x_0y_0z_0$ is located at the rotation center O with the x_0-axis passing through point Q, the midpoint of arc link B_1B_2, the z_0-axis is perpendicular to the plane where the arc link B_1B_2 lies on, and y_0-axis is defined by right hand rule.

As shown in Fig. 2, a global coordinate system O-$x_0y_0z_0$ is located at the rotation center O with the x_0-axis passing through point Q, the midpoint of arc link B_1B_2, the z_0-axis is perpendicular to the plane where the arc link B_1B_2 lies on, and y_0-axis is defined by right hand rule. the parameter θ_{ij}, where ij = 21, 32, 43, 54, 65, 61, 74, 87, 81, represent the angle between the two plane that the two adjacent links lying on. Looking at the rotation center along the revolute axis, the positive direction is counterclockwise. Due to the characteristics of the spherical mechanism that each revolute axis intersects at the rotation center O, the parameter α_i and d_{ij} equals zero, where ij =21, 32, 43, 54, 65, 61, 74, 87, 81. The i-th local coordinate systems are also located at the rotation center O. The x_i-axis along with each revolute axis, where x_1 coincides with x_9, x_2 coincides with x_{10}, x_3 coincides with x_7, x_5 coincides with x_{11}, x_8 coincides with x_{12}. The z_i-axis is perpendicular to the plane where the i-th link lying on and the y_i-axis is defined by right hand rule.

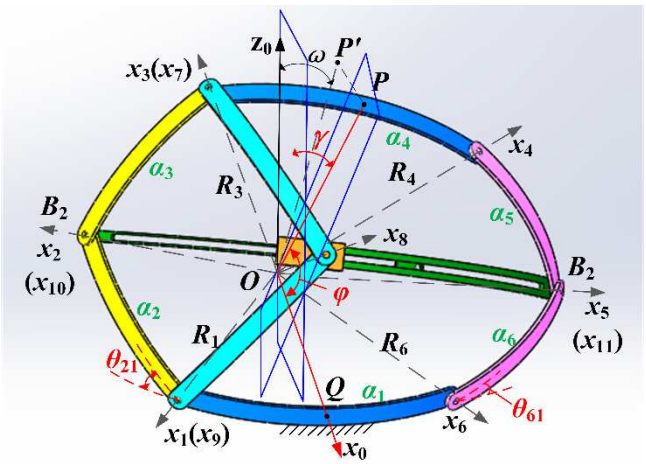

Fig . 2 Kinematic model and parameter representation of the 2-DOF SPM

Because this mechanism has two DOFs, the configuration can be represented by two angles φ and γ, where φ represents the angle between the vector ***OP*** and x_0-axis, and γ represents the angle between the mid-perpendicular plane of the end effector and the plane O-x_0z_0. Designate point P as the output reference point of the mechanism, which is the middle point of arc link B_3B_4. And the driving parameters of the mechanism are θ_{21} and θ_{61}.

In the inverse kinematics, the driving parameters θ_{21} and θ_{61} can be solved when the configuration parameters φ and γ of the end effector are given.

2.2.2 Description of the configuration

Suppose each link moves on a spherical surface with a radius R, and the position of outputs reference point P can be described by angle φ and ω:

$$\boldsymbol{P}=\begin{bmatrix}x\\y\\z\end{bmatrix}=R\begin{bmatrix}\cos\varphi\\\sin\varphi\sin\omega\\\sin\varphi\cos\omega\end{bmatrix} \tag{2}$$

where ω is the angle between the plane OPQ and the plane O-x_0z_0, which also represents the angle between the projection of vector $\boldsymbol{OP}$ on the plane O-y_0z_0 and the positive direction of z_0-axis. The relationship between γ and ω can be derived from spherical triangle PQM and MNQ. According to the characteristics of the spherical mechanism and the knowledge of spherical trigonometry[31], the relevant parameters are expressed in Fig. 3 for a clear observation.

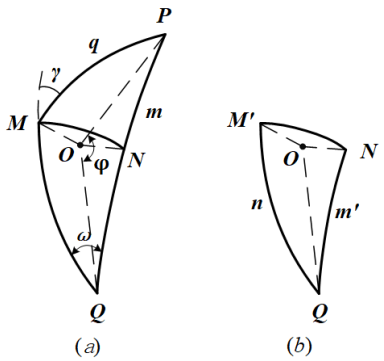

Fig. 3. Schematic of spherical triangle PQM (a) and MNQ(b)

The point M in Fig. 3(a) is the intersection point of the arc MQ (intersecting line of the mid-perpendicular plane of the end effector and spherical surface) and arc MP (intersecting line of the plane O-x_0z_0 and spherical surface), and the point M' in Fig. 3(b) is the same point with M for convenient description. The point N is the midpoint of the arc PQ (intersecting line of the plane passing through the two lines OP and OQ and spherical surface), that is, the arc MN is the intersecting line of the midplane and spherical surface.

According to the spherical triangular sine theorem, from the spherical triangle $M'NQ$ shown in Fig. 3(b) it can be derived that:

$$\frac{\sin\angle M'}{\sin\angle m'}=\frac{\sin\angle N}{\sin\angle n} \tag{3}$$

Similarly, it is available in a spherical triangle PQM shown in Fig. 3(a):

$$\frac{\sin\angle Q}{\sin\angle q}=\frac{\sin\angle M}{\sin\angle m} \tag{4}$$

In the two formulas above, $\angle M$=180°-γ, $\angle M'$=$\angle M$/2, $\angle m$=φ, $\angle m'$=$\angle m$/2, $\angle q$=$\angle n$, and $\angle N$=90°.

It can be derived from Eq. (3) and Eq. (4) that:

$$\omega=\arcsin\frac{\sin(180-\gamma)\sin\dfrac{\varphi}{2}}{\sin\dfrac{180-\gamma}{2}\sin\varphi} \tag{5}$$

2.2.3 Solutions of coordinates with configuration parameters

The trajectory of the point B_2 in the global coordinate system O-$x_0y_0z_0$ is determined by a spherical surface and a plane. As shown in Fig. 4, the radius of the spherical surface is OB_1 and the center is O. The plane is vertical to vector OB_1 and passing through the line B_2B_2'. The trajectory equation is:

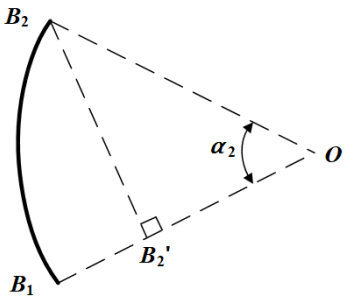

Fig. 4. Front view of link B_1B_2

Therefore, the coordinate of $B_2=[x_2\ y_2\ z_2]^{\mathrm{T}}$ in the global coordinate system O-$x_0y_0z_0$, can be obtained by Eq. (6) and Eq. (7). And the coordinate of $B_5=[x_5\ y_5\ z_5]^{\mathrm{T}}$ in the global coordinate system O-$x_0y_0z_0$, can be obtained in the similar way.

$$\begin{cases} x^2+y^2+z^2=R^2 \\ (\cos\varphi-1)\cdot x+\sin\varphi\sin\omega\cdot y+\sin\varphi\cos\omega\cdot z=0 \end{cases} \tag{6}$$

$$\begin{cases} x^2+y^2+z^2=R^2 \\ \cos\dfrac{\alpha_1}{2}\cdot x-\sin\dfrac{\alpha_1}{2}\cdot y=R\cos\alpha_2 \end{cases} \tag{7}$$

2.2.4 Solutions of coordinates with driving parameters

The coordinates of B_2 and B_5 can also be derived by D-H link parameters.

${}^{i-1}_{i}\boldsymbol{T}$ is a forward transformation matrix[32] between the adjacent local i-th and (i-1)th coordinate system, which is the coordinate transformation from i-th link to (i-1)-th link, it can be obtained by the following equation:

$${}^{i-1}_{i}\boldsymbol{T}=\mathrm{Rot}(z,\alpha_i)\mathrm{Trans}(0,0,a_i)\mathrm{Trans}(\alpha_{ij},0,0)\mathrm{Rot}(x,\theta_{ij}) \tag{8}$$

${}^{i}_{i-1}\boldsymbol{T}$ is an inverse transformation matrix between the adjacent local i-th and (i-1)th coordinate system, which is the coordinate transformation from (i-1)-th link to i-th link, and is the transpose matrix of ${}^{i-1}_{i}\boldsymbol{T}$. Then, it can be derived that:

$${}^{i}_{i-1}\boldsymbol{T}={}^{i-1}_{i}\boldsymbol{T}^{-1}={}^{i-1}_{i}\boldsymbol{T}^{\mathrm{T}} \tag{9}$$

The coordinates of revolute joints B_2 and B_5 in the global coordinate system O-$x_0y_0z_0$ can be obtained from Eq. (8) and Eq. (9):

$$\boldsymbol{b_{20}}={}^{1}_{0}\boldsymbol{T}\cdot{}^{2}_{1}\boldsymbol{T}\cdot\boldsymbol{b_{22}}=\begin{bmatrix}x_2 & y_2 & z_2\end{bmatrix}^{\mathrm{T}} \tag{10}$$

$$\boldsymbol{b_{50}}={}^{6}_{0}\boldsymbol{T}\cdot{}^{5}_{6}\boldsymbol{T}\cdot\boldsymbol{b_{55}}=\begin{bmatrix}x_5 & y_5 & z_5\end{bmatrix}^{\mathrm{T}} \tag{11}$$

where $\boldsymbol{b_{22}}=[R \quad 0 \quad 0]^{\mathrm{T}}$, $\boldsymbol{b_{55}}=[R \quad 0 \quad 0]^{\mathrm{T}}$ are the coordinates of revolute joints B_2 and B_5 in the local coordinate system O-$x_2y_2z_2$ respectively.

Derived from the coordinate of $B_2=[x_2\ y_2\ z_2]^{\mathrm{T}}$ and Eq. (10):

$$\theta_{21}=\arcsin\frac{z_2}{R\sin\alpha_2} \tag{12}$$

Derived from the coordinate of $B_2=[x_5\ y_5\ z_5]^{\mathrm{T}}$ and Eq. (11):

$$\theta_{61}=\arcsin\frac{z_5}{R\sin\alpha_6} \tag{13}$$

In the two equations above, z_2 and z_5 both have two solutions ($z_2<\pi/2$, $z_2>\pi/2$, $z_5<\pi/2$ and $z_5>\pi/2$), which means one position corresponds to four sets of solutions. The four initial configurations with different arrangements of the drive links are shown in Fig.5. Select the initial configurations in Fig.5(*a*) when analyzing the kinematics characteristic of the spherical mechanism.

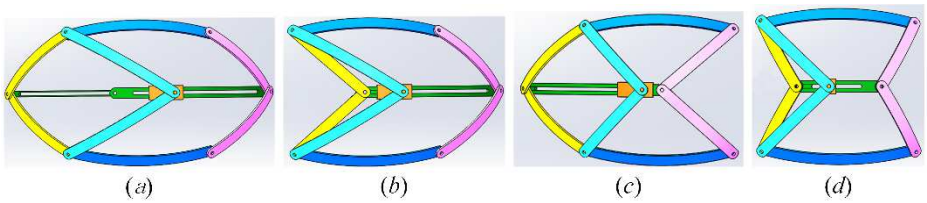

Fig. 2. Four initial configurations with different arrangements of the drive links

2.3 Forward Kinematics of the SPM

Given the driving parameters θ_{21} and θ_{61}, the solution of the configuration parameters φ and γ can be figured out, that is, the forward kinematics of the spherical mechanism. And the normal vector of the median plane is obtained by Eqs. (10) and (11):

$$\boldsymbol{b_{20}}\times\boldsymbol{b_{50}}=[r\cdot\boldsymbol{i} \quad t\cdot\boldsymbol{j} \quad s\cdot\boldsymbol{k}]^{T} \tag{14}$$

where $r=R^2\sin\alpha_6\sin\theta_{61}(\sin\frac{\alpha_1}{2}\cos\alpha_2+\cos\frac{\alpha_1}{2}\sin\alpha_2\cos\theta_{21})-$

$$R^2\sin\alpha_2\sin\theta_{21}(\sin\frac{\alpha_1}{2}\cos\alpha_6+\cos\frac{\alpha_1}{2}\sin\alpha_6\cos\theta_{61})$$

$$s=R^2\sin\alpha_2\sin\theta_{21}(\cos\frac{\alpha_1}{2}\cos\alpha_6-\sin\frac{\alpha_1}{2}\sin\alpha_6\cos\theta_{61})-$$

$$R^2\sin\alpha_6\sin\theta_{61}(\cos\frac{\alpha_1}{2}\cos\alpha_2+\sin\frac{\alpha_1}{2}\sin\alpha_2\cos\theta_{21})$$

$$t=-R^2(\cos\alpha_6\sin\alpha_2\cos\theta_{21}-\cos\alpha_2\sin\alpha_6\cos\theta_{61})$$

The equation of the mid-plane can be described by:

$$r\cdot x+s\cdot y+t\cdot z=0 \tag{15}$$

The midpoint of the fixed link $\boldsymbol{Q}=[R\ 0\ 0]^{\mathrm{T}}$ and point $\boldsymbol{P}=[x\ y\ z]^{\mathrm{T}}$ are symmetric with respect to the mid-plane. The intersection point of the line PQ and the mid-plane is $\boldsymbol{H}=[x_h\ y_h\ z_h]^{\mathrm{T}}$. Assuming that

$x_h - R/r = y_h/s = z_h/t = k$, the coordinate of the outputs reference point *P* can be obtained from the symmetrical characteristic of the mechanism:

$$\begin{cases} x = 2x_h - R \\ y = 2y_h \\ z = 2z_h \end{cases} \tag{16}$$

It can be obtained by the spherical triangular cosine theorem from the spherical triangle *M'NQ* in Fig. 3(b) that:

$$\cos\angle M' = -\cos\angle N\cos\angle Q + \sin\angle N\sin\angle Q\cos\angle m' \tag{17}$$

According to Fig. 3(a), the configuration parameters can be obtained by Eqs. (2), (16) and (17):

$$\begin{cases} \varphi = \arccos\dfrac{x}{R} \\ \gamma = 180° - 2\arccos(\sin(\arctan\dfrac{y}{z})\cos(\dfrac{1}{2}\arccos\dfrac{x}{R})) \end{cases} \tag{18}$$

2.4 Jacobian Matrix Analysis

By taking the derivative of Eq. (2) with respect to time, the following equation can be obtained:

$$\dot{\boldsymbol{P}} = \begin{bmatrix} \dot{x} \\ \dot{y} \\ \dot{z} \end{bmatrix} = \begin{bmatrix} -R\sin\varphi & 0 \\ R\cos\varphi\sin\omega & R\sin\varphi\cos\omega \\ R\cos\varphi\cos\omega & -R\sin\varphi\sin\omega \end{bmatrix} \begin{bmatrix} \dot{\varphi} \\ \dot{\omega} \end{bmatrix} \tag{19}$$

From the symmetrical characteristic of the mechanism, we can know that:

$$\begin{cases} \overrightarrow{OB_2}\cdot\overrightarrow{OP} = \boldsymbol{b}_{20}\cdot\boldsymbol{P} = R^2\cos\angle QOB_2 \\ \overrightarrow{OB_5}\cdot\overrightarrow{OP} = \boldsymbol{b}_{50}\cdot\boldsymbol{P} = R^2\cos\angle QOB_5 \end{cases} \tag{20}$$

Take the derivative each side of Eq. (20) with respect to time, the following equation can be obtained:

$$\begin{cases} \dot{\boldsymbol{b}}_{20}\cdot\boldsymbol{P} + \boldsymbol{b}_{20}\cdot\dot{\boldsymbol{P}} = R^2\sin\alpha_2\sin\dfrac{\alpha_1}{2}\sin\theta_{21}\cdot\dot{\theta}_{21} \\ \dot{\boldsymbol{b}}_{50}\cdot\boldsymbol{P} + \boldsymbol{b}_{50}\cdot\dot{\boldsymbol{P}} = R^2\sin\alpha_6\sin\dfrac{\alpha_1}{2}\sin\theta_{61}\cdot\dot{\theta}_{61} \end{cases} \tag{21}$$

where $\dot{\boldsymbol{b}}_{20} = \begin{bmatrix} \dot{x}_2 & \dot{y}_2 & \dot{z}_2 \end{bmatrix}^{\mathrm{T}}$, $\dot{\boldsymbol{b}}_{50} = \begin{bmatrix} \dot{x}_5 & \dot{y}_5 & \dot{z}_5 \end{bmatrix}^{\mathrm{T}}$.

It can be derived by Eqs. (10), (11) and (19) that:

$$\begin{bmatrix} \dot{\theta}_{21} & \dot{\theta}_{61} \end{bmatrix}^{\mathrm{T}} = \boldsymbol{J}\begin{bmatrix} \dot{\varphi} & \dot{\omega} \end{bmatrix}^{\mathrm{T}} \tag{22}$$

$\boldsymbol{J}$ in Eq. (22) is the inverse kinematics Jacobian matrix.

$$\boldsymbol{J} = \begin{bmatrix} e_2/d_2 & f_2/d_2 \\ e_6/d_6 & f_6/d_6 \end{bmatrix} \tag{23}$$

where $d_i = D_i(x-R) + E_i y + F_i z$;

$$e_i = -R(-x_j \sin\varphi + y_j \cos\varphi \sin\omega + z_j \cos\varphi \cos\omega)$$

$$f_i = -R(y_j \sin\varphi \cos\omega - z_j \sin\varphi \sin\omega)$$

$$D_i = R\sin\alpha_i \sin\frac{\alpha_1}{2}\sin\theta_{i1};$$

$$E_i = R\sin\alpha_i \sin\frac{\alpha_1}{2}\cos\theta_{i1};$$

$F_i = R\sin\alpha_i \cos\theta_{i1}$ (i=2, 6, when i=2 and 6, j=2 and 5 respectively).

2.5 Verification of Kinematic Analysis

Verify the correctness of Jacobian matrix and the forward kinematics by comparing the numerical solution obtained by Eqs. (22) and (23) and the measurement obtained by 3D model, when giving two tiny value as inputs[33].

Table 1. Verification of the Jacobian matrix

Institutional parameters of the initial configuration	Tiny input$\theta_{21;}\ \theta_{61}$(°)	The theoretical value of Jacques φ, γ (×10^{-3}°/s)	The value of CAD model Δφ, Δγ (×10^{-3}°/s)
θ_{21}=14°	0.001	3.4397	3.4417
θ_{61}=23°	0.002	-0.3657	-0.3505
φ=59.0786°	-0.003	0.9701	0.8857
λ=-4.7420°	0.004	-3.6240	-3.6368
θ_{21}=31°	0.001	-1.1911	-1.2617
θ_{61}=12°	-0.002	1.5686	1.6108
φ=64.9472°	-0.003	1.4643	1.6035
λ=9.2984°	0.004	-3.5059	-3.5913

Four sets of data under two general configurations are given, as shown in Table 1. Then, the correctness of inverse kinematic model is verified in the same way, which means the correctness of the kinematics analysis of the 2DOF SPM.

3 Workspace Analysis

Due to the interference of the mechanism, the reference point *P* of the effector can't reach every point on the spherical surface. As shown in Fig. 1, suppose the width of each link of the mechanism is 8mm, the effective radius is R=200mm, that is, *OP*=*OQ*=200mm, and α_1=α_4=60°, α_2=α_3=α_5=α_6=40°, α_7=α_8=50°.

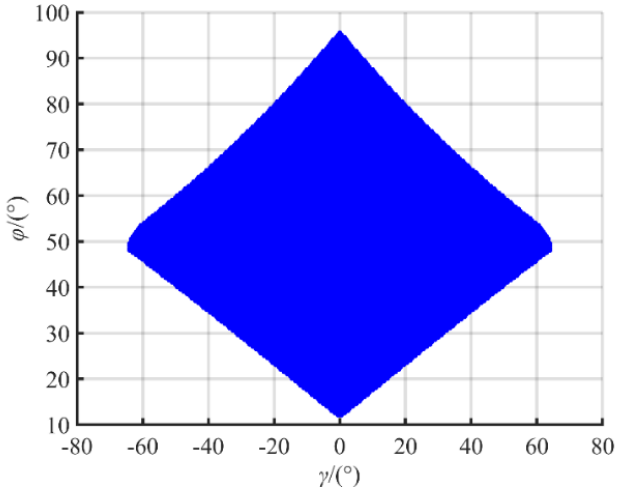

Fig. 6. Workspace of the spherical mechanism

Table 2. Limited configuration parameters of the spherical mechanism

	Limited configuration 1	Limited configuration 2	Limited configuration 3	Limited configuration 4
φ / (°)	49.8502°	49.8502°	95.8430°	11.5519°
λ / (°)	-67.5085°	67.5085°	0°	0°
configuration of the mechanism	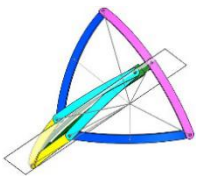	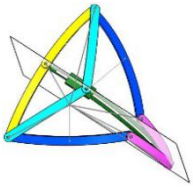	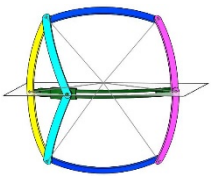	

To avoid interference, considering the width of the links, assume that the angle between the rotation axes OB_1 and OB_3 and the angle between OB_4 and OB_6 are not less than 10°. The workspace of the mechanism in Fig. 6 can be obtained according to the inverse kinematics and the interference condition. The specific limited configuration and corresponding position parameters of the mechanism are shown in Table 2.

4 Equivalent Rotation Characteristics of the Mechanism

4.1 Equivalent Rotation Characteristics

The end effector of the 2DOF SPM can realize continuous rotation around the axis that passes through the rotation center and lies on the mid-plane during the moving process. Moreover, the 2DOF SPM also has the following motion properties: The end effector can move from the initial position to the final position around a fixed axis no matter how the revolute axis changes in the motion process, called equivalent rotation of the mechanism.

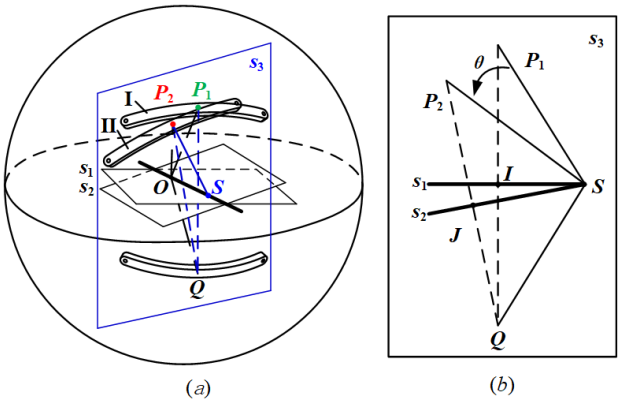

Fig. 7 Schematic diagram of the initial and final configuration (*a*) and front view of plane s_3 (*b*)

As the simplified motion model shown in Fig. 7(*a*), the end effector moves from position I to position II, and the mid-planes at the initial and final positions are v_1 and v_2, the symmetric points of Q about the mid-plane are P_1 and P_2, respectively. The line l is the intersection line of the two mid-planes, and the axis of the equivalent rotation[34]. For a clearly obversion, a plane s_3 is set, which passes through line OP_1 and is perpendicular to line l, as shown in Fig. 7(*b*). S is the intersection point of the line l and the plane s_3. I is the intersection point of line QP_1 and plane s_1. J is the intersection point of line QP_2 and plane s_2.

4.2 Motion Planning of the Equivalent Rotation

As shown in Fig. 7(*a*), the two parameters φ_1 and γ_1 of the initial configuration of the mechanism and the two parameters φ_2 and γ_2 of the final configuration are given. The coordinates of output reference point can be obtained by Eq. (2). The equation of axis l, which is the intersection line of the two mid-planes, can be obtained by Eq. (15). The equation of plane s_3, which is passing through lines QP_1 and QP_2 , can be obtained according to the structural characteristics. And the coordinates of the point S can be obtained by the equations of axis l and plane s_3.

Then the rotated angle of the output reference point P can be derived that:

$$\theta = \arccos\left(\frac{\boldsymbol{SP_1}\cdot\boldsymbol{SP_2}}{|\boldsymbol{SP_1}|\cdot|\boldsymbol{SP_2}|}\right) \tag{24}$$

where $\boldsymbol{SP_1}=\boldsymbol{P_1}-\boldsymbol{S}$ and $\boldsymbol{SP_2}=\boldsymbol{P_2}-\boldsymbol{S}$.

The direction vector $\boldsymbol{l}=[l_x\ l_y\ l_z]^{\mathrm{T}}$ and the rotation angle θ of the end effector rotating around the axis l are already obtained, and the rotation matrix $\mathrm{R}_{(\theta)}$ can be expressed by:

$$\boldsymbol{R}_{(\theta)}=\begin{bmatrix} l_x l_x(1-\cos\theta)+\cos\theta & l_y l_x(1-\cos\theta)-l_z\sin\theta & l_z l_x(1-\cos\theta)+l_y\sin\theta \\ l_x l_y(1-\cos\theta)+l_z\sin\theta & l_y l_y(1-\cos\theta)+\cos\theta & l_z l_y(1-\cos\theta)-l_x\sin\theta \\ l_x l_z(1-\cos\theta)-l_y\sin\theta & l_y l_z(1-\cos\theta)+l_x\sin\theta & l_z l_z(1-\cos\theta)+\cos\theta \end{bmatrix} \tag{25}$$

The vector $\boldsymbol{QP_2}$ can be expressed as:

$$\boldsymbol{QP_2}=\mathbf{R}_{(\theta)}\boldsymbol{SP_1}+\boldsymbol{QS} \tag{26}$$

The coordinates of point P_2 can be obtained by the Eq. (26), and the other parameters of the mechanism can be obtained by the inverse kinematics described in Section 2.2. Thereby, the driving parameters θ_{21} and θ_{61} of the rotation process can be obtained. It provides the basis for the motion planning of the spherical mechanism.

4.3 Numerical Example of the Equivalent Rotation

As shown in Fig. 2, suppose the effective radius is R=200mm, that is, OP=OQ=200mm, and α_1=α_4=60°, α_2=α_3=α_5=α_6=40°, α_7=α_8=50°. The parameters of initial position are φ_1=75°, γ_1=-20°, and the parameters of final position are φ_2=70°, γ_2=20°. The four configurations of the mechanism from the initial position to the final position are shown in Fig. 8(a)~(d), respectively. The detailed parameters of each configuration are listed in Table 3.

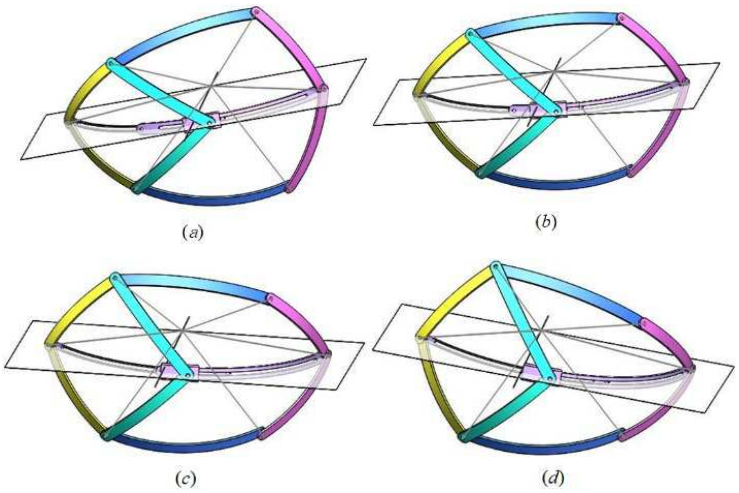

Fig. 8. Numerical example of the equivalent rotation

Table 3. Numerical calculation example of the equivalent rotation

	Configuration 1 (θ=0°)	Configuration 2 （θ=13°）	Configuration 3 （θ=26°）	Configuration 4 （θ=40.3230°）
Equation of rotation axis		$\frac{x}{-0.7933}=\frac{y}{0.1257}=\frac{z}{-0.5957}$		
Institutional configuration φ, γ	φ=75° γ=-20°	φ=74.5359° γ=--7.1049°	φ=72.9604° γ=-5.7918°	φ=70° γ=20°
Driving angle	θ_{21}=5.3391° θ_{61}=56.7404°	θ_{21}=18.3470° θ_{61}=35.3134°	θ_{21}=32.3670° θ_{61}=18.9834°	θ_{21}=49.2440° θ_{61}=3.7442°

5 Variant Mechanisms of the 2DOF SPM

Based on 3DOF planar sub-chain, a group of variant 2DOF SPMs with the same characteristics are synthesized, providing more possibilities for practical application.

In the middle of this mechanism, there are two arc prismatic joints which connect links 9, 10 and 11. Its function is to keep the lines OB_2, OB_5 and OB_8 on the same mid-plane. We can use a 3DOF planar sub-chain to provide the same constraints. In this way, we can get a group of variant 2DOF SPM without arc prismatic joints. Compared with the variation mechanism, the mechanism with arc prismatic joints really needs higher precision to ensure the motion performance of the mechanism. But its disadvantage is taking more space than the original mechanism.

There are seven different configurations of the 3DOF planar sub-chain can be obtained: [RRR], [RPR], [PRR], [RRP], [PPR], [PRP], [RPP], in which R represents revolute joint and *P* represents prismatic joint[35], and several 2DOF SPMs based on them are shown in Fig. 9.

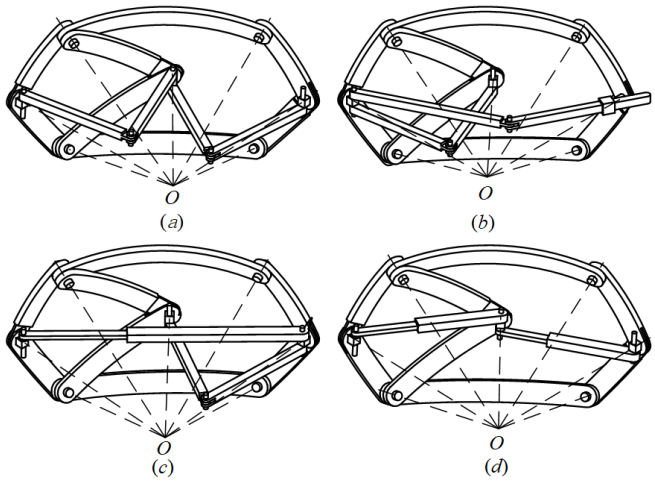

Fig. 9. Several 2DOF SPMs based on 3DOF planar sub-chain

6 Conclusions

A novel 2DOF Spherical Parallel Mechanism (SPM) is proposed. The SPM can realize continuous rotation around any line on the mid-plane which passes through the rotation center of the spherical mechanism, and the rotational axis can be fixed during the rotation process, which means any form of motion of the mechanism can be transformed to a rotation with a fixed axis.

The forward and inverse kinematics of the mechanism are solved based on D-H parameters and analytical geometry. The inverse Jacobian matrix of the 2DOF SPM is obtained by taking the derivative of the constraint equation, and its workspace is analyzed by considering the interference condition of the links. The correctness of the kinematics and motion planning of the mechanism is verified by the motion examples presented.

A group of variant 2DOF SPMs are constructed based on 3DOF planar sub-chain, that can provide more possibilities for practical application.

7 Declaration

Acknowledgements

The authors sincerely thanks to Professor Huang Zhen of Yanshan University for his critical discussion and reading during manuscript preparation.

Funding

Supported by National Natural Science Foundation of China (NSFC) under Grant No. 51775474.

Availability of data and materials

The datasets supporting the conclusions of this article are included within the article.

Authors' contributions

The author' contributions are as follows: Chen Ziming was in charge of the whole trial; Chen Xuechan and Gao Min wrote the manuscript; the remaining authors assisted with sampling and laboratory analyses.

Competing interests

The authors declare no competing financial interests.

Consent for publication

Not applicable

Ethics approval and consent to participate

Not applicable

References

[1] Luo J, Liu H, Yu S, et al. Development of an Image-based Visual Servoing for Moving Target Tracking Based on Bionic Spherical Parallel Mechanism[M]. 2014: 1633-1638.

[2] Kumar S, Bongardt B, Simnofske M, et al. Design and Kinematic Analysis of the Novel Almost Spherical Parallel Mechanism Active Ankle[J]. Journal of Intelligent & Robotic Systems, 2019, 94 (2): 303-325.

[3] Chablat D, Michel G, Bordure P, et al. Workspace analysis in the design parameter space of a 2-DOF spherical parallel mechanism for a prescribed workspace: Application to the otologic surgery[J]. Mechanism and Machine Theory, 2021, 157.

[4] Saafi H, Laribi M A, Zeghloul S. Optimal torque distribution for a redundant 3-RRR spherical parallel manipulator used as a haptic medical device[J]. Robotics and Autonomous Systems, 2017, 89: 40-50.

[5] Bian B, Wang L. Design, Analysis, and Test of a Novel 2-DOF Spherical Motion Mechanism[J]. Ieee Access, 2020, 8: 53561-53574.

[6] Leal-Naranjo J-A, Wang M, Paredes-Rojas J-C, et al. Design and kinematic analysis of a new 3-DOF spherical parallel manipulator for a prosthetic wrist[J]. Journal of the Brazilian Society of Mechanical Sciences and Engineering, 2019, 42 (1).

[7] Bai S. Optimum design of spherical parallel manipulators for a prescribed workspace[J]. Mechanism and Machine Theory, 2010, 45 (2): 200-211.

[8] Bonev I, Gosselin C. Singularity loci of spherical parallel mechanisms[M]. 2005. 2005: 2957-2962.

[9] Gosselin C, Angeles J. A Global Performance Index for the Kinematic Optimization of Robotic Manipulators[J]. ASME Journal of Mechanical Design, 1991, 113: 220-226.

[10] Gosselin C. Stiffness Mapping for Parallel Manipulators[J]. Robotics and Automation, IEEE Transactions on, 1990, 6: 377-382.

[11] Danaei B, Arian A, Masouleh M T, et al. Dynamic modeling and base inertial parameters determination of a 2-DOF spherical parallel mechanism[J]. Multibody System Dynamics, 2017, 41 (4): 367-390.

[12] Gosselin C, Hamel J F. The Agile Eye: A High-Performance Three-Degree-of-Freedom Camera-Orienting Device[M]. 1. 1994: 781-786 vol.1.

[13] Yu J, Wu K, Zong G, et al. A Comparative Study on Motion Characteristics of Three Two-Degree-of-Freedom Pointing Mechanisms[J]. Journal of Mechanisms and Robotics-Transactions of the Asme, 2016, 8 (2).

[14] Bajaj N M, Spiers A J, Dollar A M. State of the Art in Artificial Wrists: A Review of Prosthetic and Robotic Wrist Design[J]. Ieee Transactions on Robotics, 2019, 35 (1): 261-277.

[15] Ouerfelli M, Kumar V. Optimization of a Spherical Five-Bar Parallel Drive Linkage[J]. Journal of Mechanical Design - J MECH DESIGN, 1994, 116.

[16] Cervantes-Sanchez J J, Hernandez-Rodriguez J C, Gonzalez-Galvan E J. On the 5R spherical, symmetric manipulator: workspace and singularity characterization[J]. Mechanism and Machine Theory, 2004, 39 (4): 409-429.

[17] Zhang L-J, Niu Y-W, Li Y-Q, et al.: Analysis of the workspace of 2-DOF spherical 5R parallel manipulator,2006 Ieee International Conference on Robotics and Automation,2006: 1123-1128.

[18] Li Y, Zhang L, Niu Y. Dynamic analysis of spherical 2-DOF parallel manipulator with actuation redundancy[J]. 2011.

[19] Zhang L J, Li Y Q, Guo Y Q. Dynamic analysis of spherical 5R parallel manipulator[C]. International Conference on Mechatronics & Automation, 2009.

[20] Yongquan Li L Z, Yuewei Niu. Dynamic Analysis of Spherical 2-DOF Parallel Manipulator with Actuation Redundancy[J]. 2011 IEEE Int. Conf. Mech. Autom, 2011: 1350-1355.

[21] Zhang L-J, Li Y-Q, Shi W-Y. Parameter Optimum Design of Spherical 2-DOF Parallel manipulator with Actuation Redundancy[M]. 2009: 1499-1504.

[22] Yu J J, Dong X, Pei X, et al. MOBILITY AND SINGULARITY ANALYSIS OF A CLASS OF 2-DOF ROTATIONAL PARALLEL MECHANISMS USING A VISUAL GRAPHIC APPROACH[M]. 2012: 1027-+.

[23] Dong X, Yu J, Chen B, et al. Geometric Approach for Kinematic Analysis of a Class of 2-DOF Rotational Parallel Manipulators[J]. Chinese Journal of Mechanical Engineering, 2012, 25 (2): 241-247.

[24] Chen Bin Z G, Yu Jingjun , Dong Xin. Dynamic modeling and analysis of 2-DOF quasi-sphere parallel platform[J]. Chinese J. Mech. Eng, 2013, 49 (13): 24-31.

[25] Xu Y, Zhang D, Wang M, et al. Type synthesis of two-degrees-of-freedom rotational parallel mechanism with two continuous rotational axes[J]. Chinese Journal of Mechanical Engineering, 2016, 29 (4): 694-702.

[26] Tae-Uk K, Yonghwan O, Ieee: Design of Spatial Adaptive Fingered Gripper Using Spherical Five-Bar Mechanism,2014 International Conference on Advanced Mechatronic Systems,2014: 145-150.

[27] Essomba T, Linh Nguyen V. Kinematic analysis of a new five-bar spherical decoupled mechanism with two-degrees of freedom remote center of motion[J]. Mechanism and Machine Theory, 2018, 119: 184-197.

[28] Cao W-A, Xu S-J, Rao K, et al. Kinematic Design of a Novel Two Degree-of-Freedom Parallel Mechanism for Minimally Invasive Surgery[J]. Journal of Mechanical Design, 2019, 141 (10).

[29] Alamdar A, Farahmand F, Behzadipour S, et al. A geometrical approach for configuration and singularity analysis of a new non-symmetric 2DOF 5R Spherical Parallel Manipulator[J]. Mechanism and Machine Theory, 2020, 147.

[30] Ding W, Yao Y-A: Self-crossing Motion Analysis of a Novel Inpipe Parallel Robot with Two Foldable Platforms, Corves B, Lovasz E C, Husing M,editor,Mechanisms, Transmissions and Applications,2015: 221-229.

[31] Shor J B. Kinematics of spherical mechanisms[M]. Cambridge university press,1988.

[32] Craig J. Introduction To Robotics Mechanics & Control[M]. 1989.

[33] Cuan-Urquizo E, Rodriguez-Leal E. Kinematic analysis of the 3-CUP parallel mechanism[J]. Robotics and Computer-Integrated Manufacturing, 2013, 29 (5): 382-395.

[34] Zhao C, Chen Z, Li Y, et al. Motion Characteristics Analysis of a Novel 2R1T 3-UPU Parallel Mechanism[J]. Journal of Mechanical Design, 2020, 142 (1).

[35] Chen Z, Cao W A, Huang Z. Type Synthesis of 3-DOF Rotational Parallel Mechanisms With No Intersecting Axes[C]. Asme International Design Engineering Technical Conferences & Computers & Information in Engineering Conference, 2012.

Figures

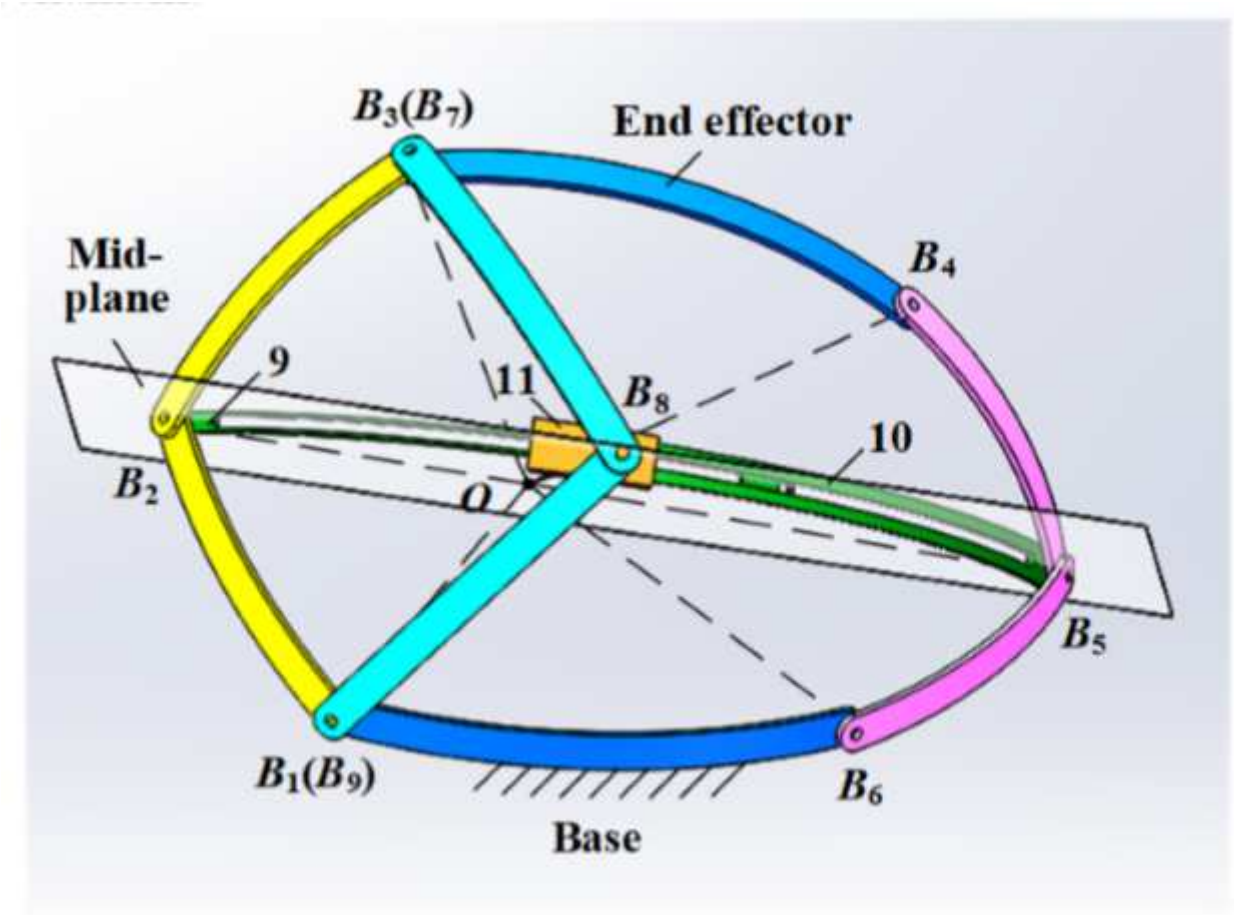

Figure 1

Schematic diagram of the 2-DOF SPM

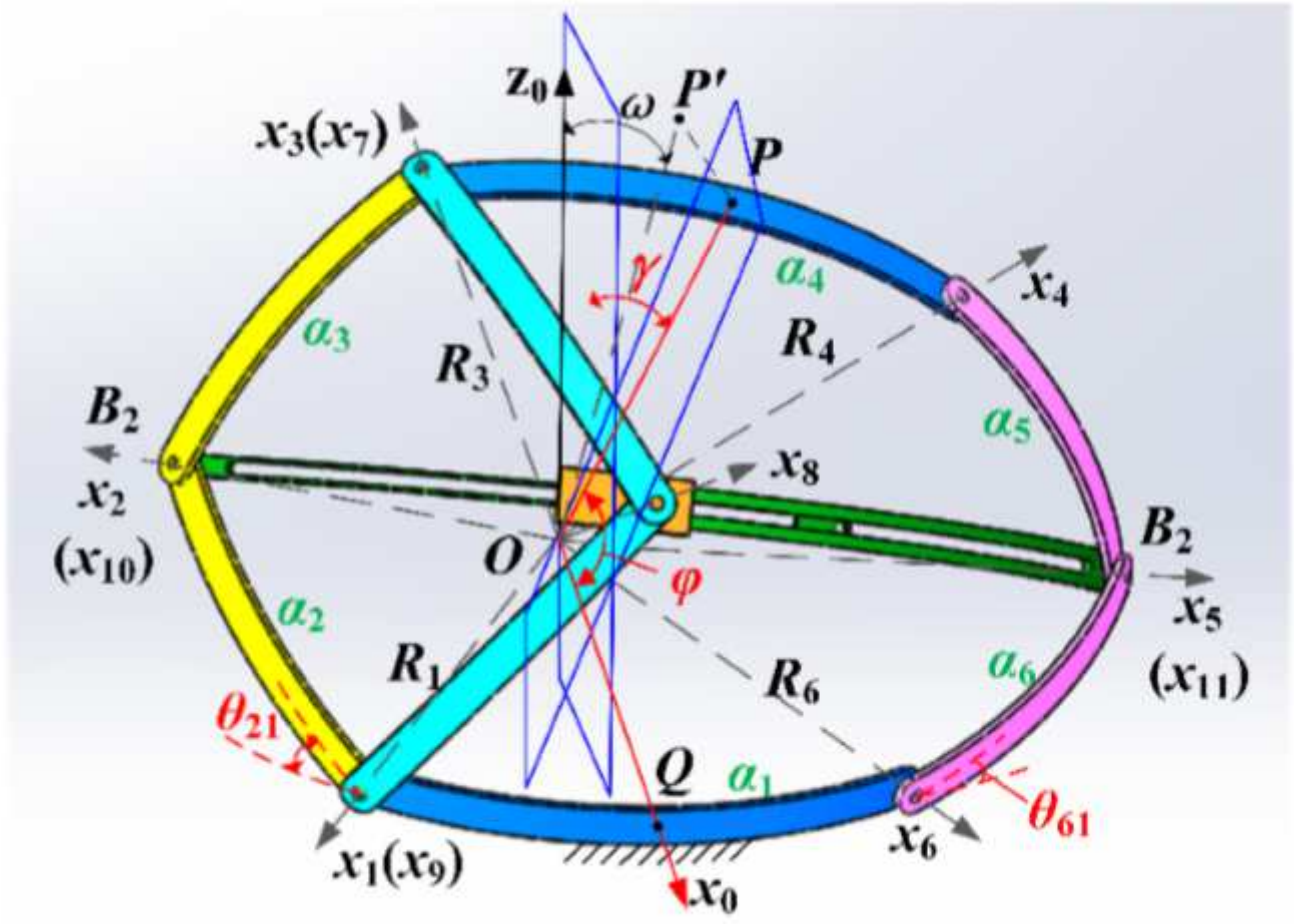

Figure 2

Kinematic model and parameter representation of the 2-DOF SPM

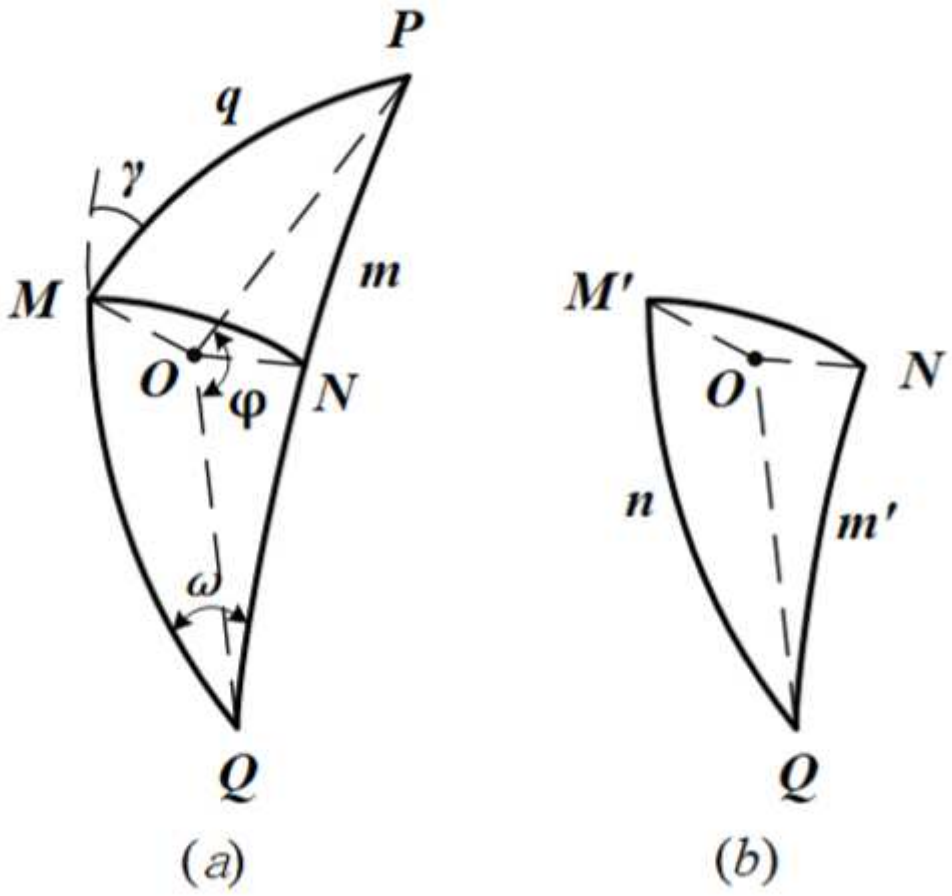

Figure 3

Schematic of spherical triangle PQM (a) and MNQ(b)

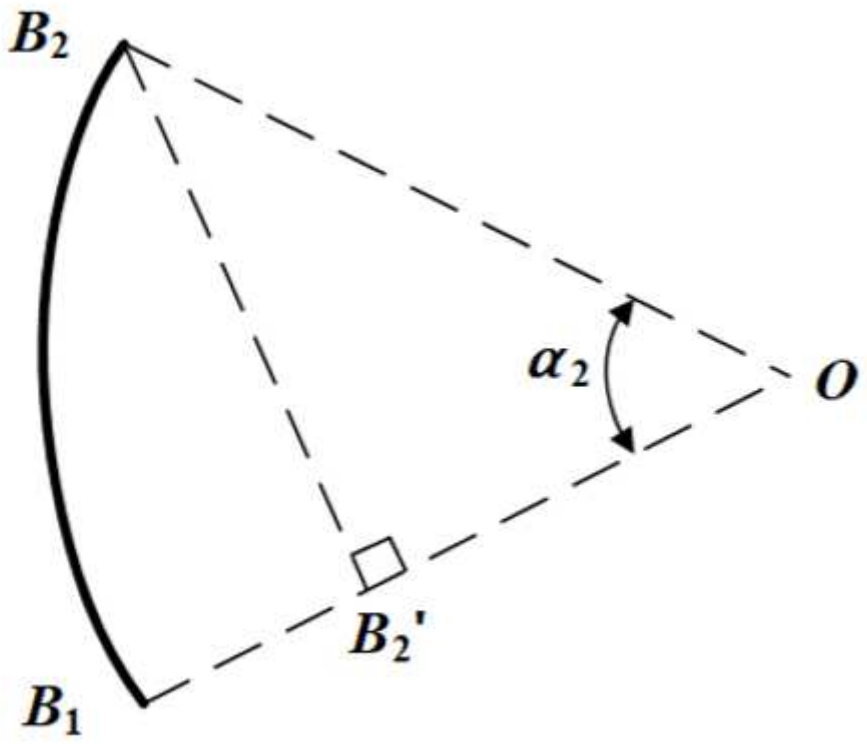

Figure 4

Front view of link B1B2

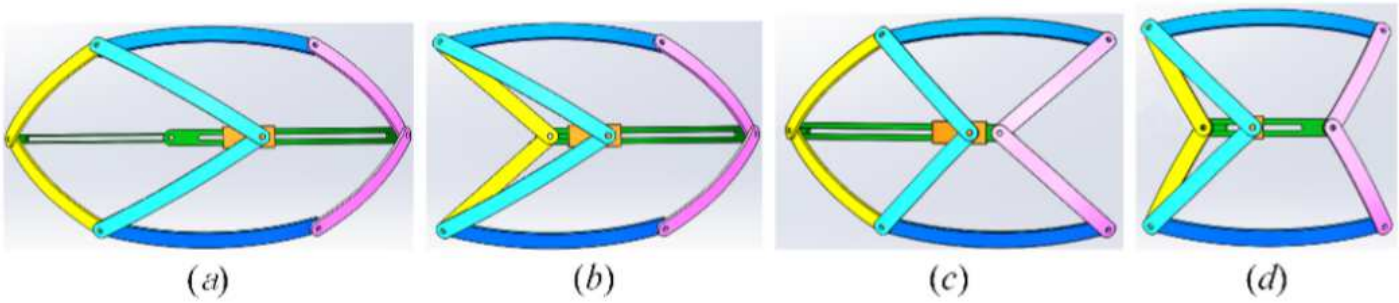

Figure 5

Four initial configurations with different arrangements of the drive links

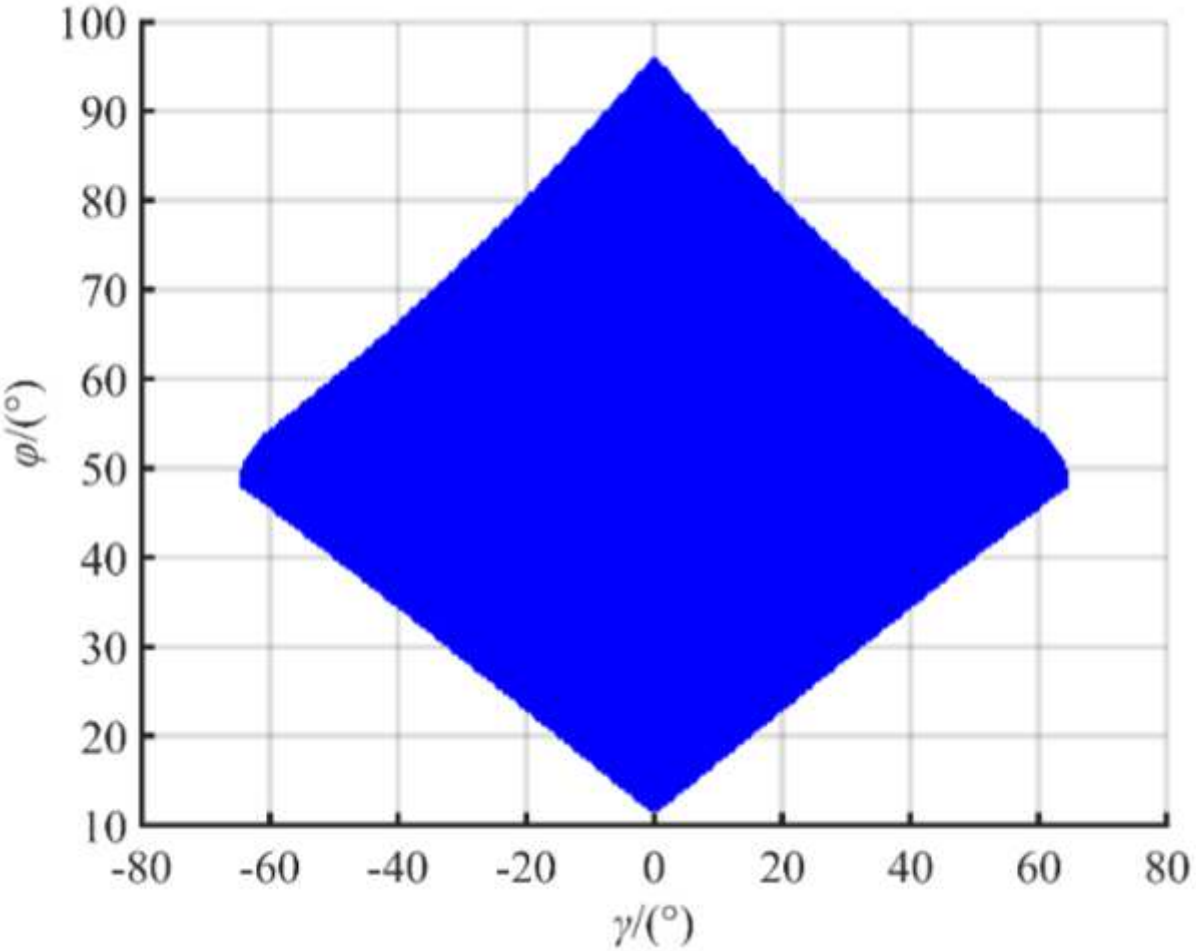

Figure 6

Workspace of the spherical mechanism

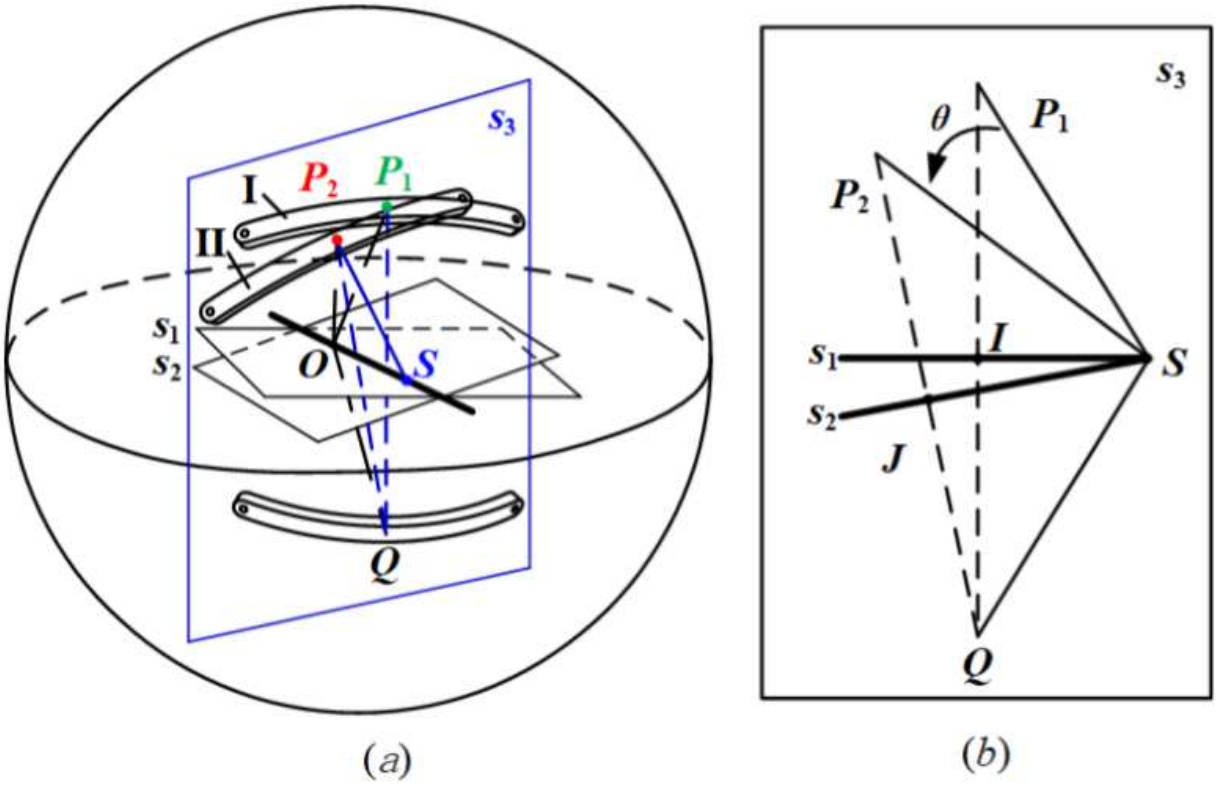

Figure 7

Schematic diagram of the initial and final configuration (a) and front view of plane s3 (b)

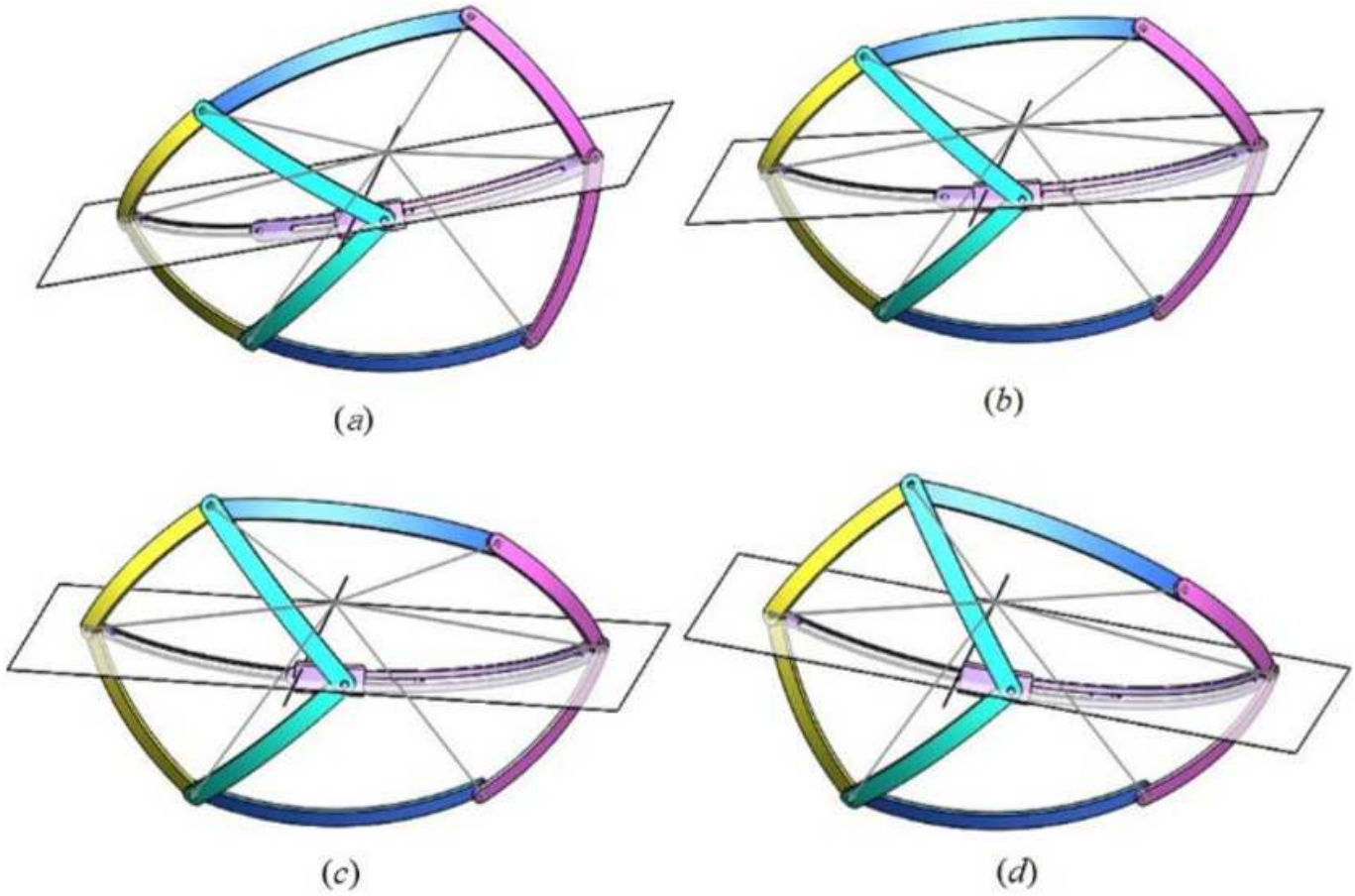

Figure 8

Numerical example of the equivalent rotation

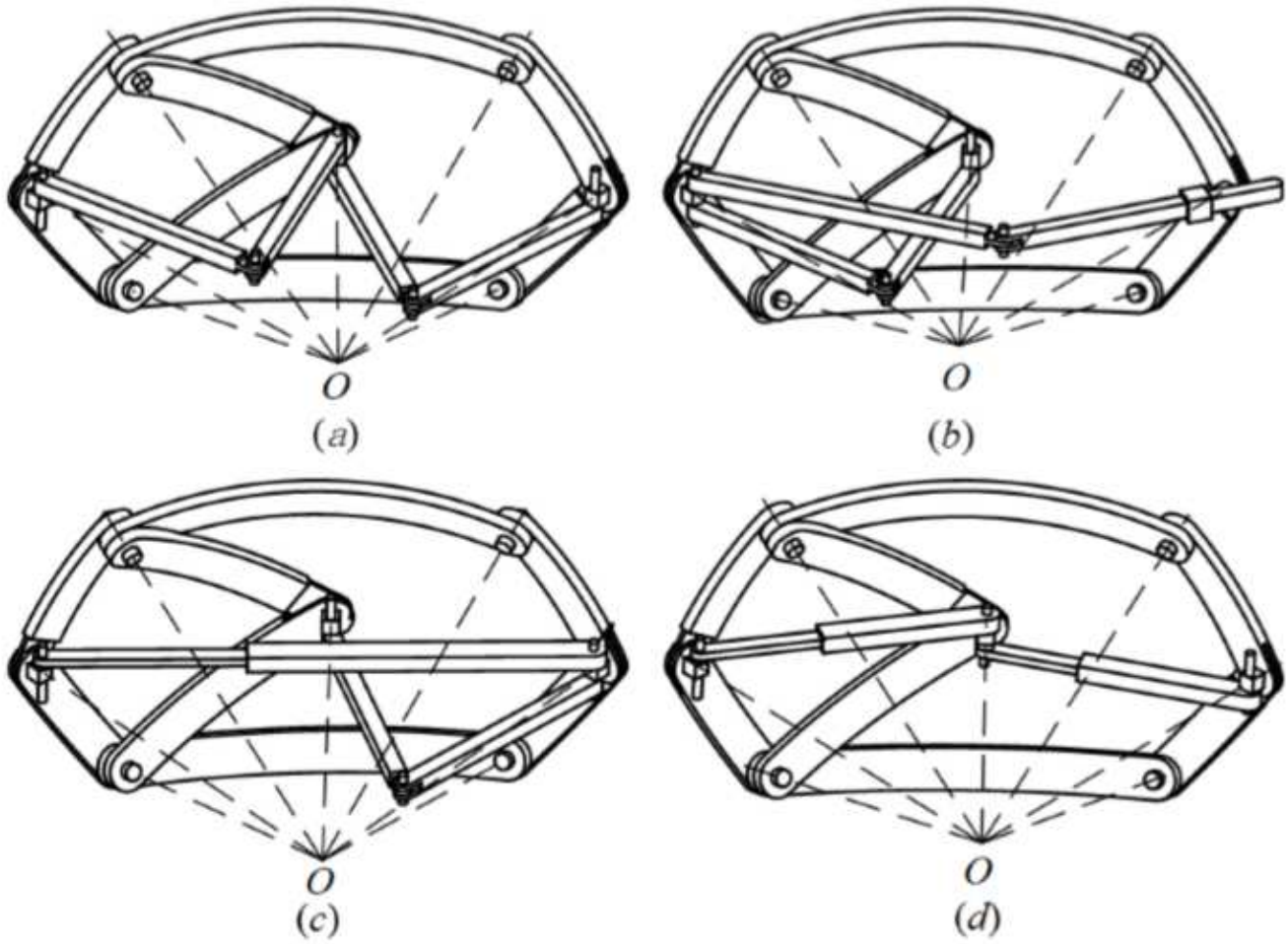

Figure 9

Several 2DOF SPMs based on 3DOF planar sub-chain